

Document downloaded from:

<http://hdl.handle.net/10251/50329>

This paper must be cited as:

Gomis Hilario, O.; Santamaría-Pérez, D.; Vilaplana Cerda, Rl.; Luna Molina, R.; Sans, JA.; Manjón Herrera, FJ.; Errandonea, D.... (2014). Structural and elastic properties of defect chalcopyrite HgGa₂S₄ under high pressure. *Journal of Alloys and Compounds*. 583:70-78. doi:10.1016/j.jallcom.2013.08.123.



The final publication is available at

<http://dx.doi.org/10.1016/j.jallcom.2013.08.123>

Copyright Elsevier

28

Abstract

29 In this work, we focus on the study of the structural and elastic properties of
30 mercury digallium sulfide (HgGa_2S_4) at high pressures. This compound belongs to the
31 family of AB_2X_4 ordered-vacancy compounds and exhibits a tetragonal defect
32 chalcopyrite structure. X-ray diffraction measurements at room temperature have been
33 performed under compression up to 15.1 GPa in a diamond anvil cell. Our
34 measurements have been complemented and compared with *ab initio* total energy
35 calculations. The axial compressibility and the equation of state of the low-pressure
36 phase of HgGa_2S_4 have been experimentally and theoretically determined and compared
37 to other related ordered-vacancy compounds. The pressure dependence of the
38 theoretical cation-anion and vacancy-anion distances and compressibilities in HgGa_2S_4
39 are reported and discussed in comparison to other related ordered-vacancy compounds.
40 Finally, the pressure dependence of the theoretical elastic constants and elastic moduli
41 of HgGa_2S_4 has been studied. Our calculations indicate that the low-pressure phase of
42 HgGa_2S_4 becomes mechanically unstable above 13.8 GPa.

43

44 **Keywords:**

45 **A. Semiconductors**

46 **C. Equation of state**

47 **C. Elasticity**

48 **C. Mechanical properties**

49 **D. High-pressure**

50 **D. X-ray diffraction**

51

52

53 **1. Introduction**

54 Mercury digallium sulfide (HgGa_2S_4) is a tetrahedrally-coordinated
55 semiconductor of the $A^{\text{II}}B_2^{\text{III}}X_4^{\text{VI}}$ family which crystallizes at ambient conditions in the
56 tetragonal defect chalcopyrite (DC) structure (S.G. I-4, No. 82, $Z=2$) [1-3]. The
57 unbalanced number of cations (A and B) and anions (X) in tetrahedrally-coordinated
58 $A^{\text{II}}B_2^{\text{III}}X_4^{\text{VI}}$ semiconductors results in inequivalent tetrahedrally-coordinated A and B
59 cations (located in different Wyckoff sites) and in the occupation of a cation site by a
60 vacancy in an ordered and stoichiometric fashion. For this reason, these semiconductors
61 are classified as ordered-vacancy compounds (OVCs). The lack of cubic symmetry and
62 the rather strong anisotropy make OVCs suitable for many technological applications
63 [4-7].

64 HgGa_2S_4 is of considerable interest because it combines nonlinear optical
65 properties in the mid-infrared range, high non-linear susceptibility coefficients,
66 birefringence, and a wide transparency range from 0.5 to 13 μm [8-11]. This compound
67 can be used for frequency doubling, optical parametric oscillator, and optical parametric
68 amplifier in the wavelength range from 1.0 to 10 μm because the high values of laser
69 damage threshold and conversion efficiency are combined with a suitable thermal
70 conductivity and high specific heat capacity [11, 12]. In fact, the combined properties of
71 HgGa_2S_4 crystals make this compound to potentially occupy a leading position among
72 the crystals used in non-linear optical devices [11].

73 Several high-pressure (HP) studies on $A^{\text{II}}B_2^{\text{III}}X_4^{\text{VI}}$ compounds have been carried
74 out in the last years [13-34]. In particular, HP X-ray diffraction (XRD) measurements
75 have been performed on CdGa_2Se_4 [18], MnGa_2Se_4 [24], ZnGa_2Se_4 [26], CdGa_2S_4 [26],
76 CdAl_2Se_4 [25], HgAl_2Se_4 [27], CdAl_2S_4 [27], and HgGa_2Se_4 [32, 33]. However, to the
77 best of our knowledge, there is no study published on the structural and elastic

78 properties of HgGa_2S_4 under pressure. We present here HP XRD measurements up to
79 15.1 GPa and *ab initio* total energy calculations in DC- HgGa_2S_4 in order to study the
80 structural properties of the low-pressure phase of HgGa_2S_4 . In particular, its equation of
81 state (EOS) and the axial compressibilities are reported. We have also carried out
82 calculations of the elastic properties of DC- HgGa_2S_4 and have studied its mechanical
83 stability under pressure.

84

85 **2. Experimental section**

86 Single crystals of DC- HgGa_2S_4 have been grown from its constituents HgS and
87 Ga_2S_3 by chemical vapor transport method using iodine as a transport agent [35]. The
88 as-grown crystals of uniform light-yellow color represent triangular prisms with mirror
89 surfaces. Chemical and structural analyses have shown the stoichiometric composition
90 of the crystals and no spurious phases have been observed [3]. The samples used in this
91 study were already characterized at room pressure (RP) by XRD in the 2θ range of 5-
92 85° collected using a DRON-R4M diffractometer with Cu K_α radiation [3] and by
93 Raman spectroscopy [34] confirming that our sample has a DC-type structure.

94 HP angle-dispersive powder XRD experiments at room temperature have been
95 performed in a modified diamond anvil cell (DAC) with an Oxford Xcalibur
96 diffractometer. The same setup has been recently used to successfully characterize the
97 HP behavior of several sulfides and selenides [33, 36, 37]. The DAC used for the
98 experiments has an angular access of $2\theta = 25^\circ$ and diamond anvils with 500 μm of culet
99 size. The powder samples were placed in the 150 μm -diameter hole of a stainless-steel
100 gasket preindented to a thickness of 50 μm . A 4:1 methanol-ethanol mixture was used
101 as quasi-hydrostatic pressure-transmitting medium (PTM) [38, 39]. Pressure was
102 determined by the ruby fluorescence method [40] and in our experiment it has been

103 limited to 15.1 GPa to avoid the influence of deviatoric stresses and of precursor effects
104 [41] associated to the phase transitions observed in this compound [34] and in other
105 $A^{II}B_2^{III}X_4^{VI}$ OVCs between 15 and 23 GPa [18, 24-27, 32]. X-ray beam collimated to a
106 diameter of 300 μm from Mo K_α radiation ($\lambda = 0.7107 \text{ \AA}$) allowed to collect XRD
107 patterns on a 135 mm Atlas CCD detector placed at 110 mm from the sample. A small
108 phi rotation from -2 to 2° (width 2°) was used for the images collected on the Atlas
109 CCD. In this particular experiment, the CCD was placed in two different positions, at -4
110 and 4° . Taking into account this and the aforementioned phi rotation and width, the
111 total amount of frames was four. The total exposure time per image was 10 minutes,
112 being the approximate data collection time 40 minutes. Dark images were previously
113 collected with a similar exposure time. The CrysAlis software [42] was used for data
114 collection and preliminary data reduction. The observed intensities were integrated as a
115 function of 2θ in order to give conventional, one-dimensional diffraction profiles. No
116 smoothing procedure was used in the integration procedure. The indexing and
117 refinement of the powder diffraction patterns were performed using the CHEKCELL
118 [43], POWDERCELL [44], and GSAS [45, 46] program packages.

119

120 **3. Theoretical calculation details**

121 *Ab initio* total energy calculations have been carried out for DC-HgGa₂S₄ within
122 the density functional theory (DFT) using the plane-wave method and the
123 pseudopotential theory with the Vienna *ab initio* simulation package (VASP) [47]. The
124 set of plane waves employed extended up to a kinetic energy cutoff of 370 eV. The
125 generalized gradient approximation (GGA) has been used for the description of the
126 exchange-correlation energy with the PBEsol exchange-correlation prescription [48].

127 We used dense special point grids appropriate to sample the Brillouin zone (BZ) when
128 relaxing the structure at different volumes. Pressure, like other energy derivatives, is
129 obtained at the same time from the stress tensor [49]. Additional details of total energy
130 calculations in the DC structure of OVCs can be consulted in Ref. [29].

131 In order to study the mechanical properties of DC-HgGa₂S₄ by means of *ab*
132 *initio* calculations we have calculated the elastic constants, which describe the
133 mechanical properties of a material in the region of small deformations; i.e., where the
134 stress-strain relations are still linear. The elastic constants can be obtained by computing
135 the macroscopic stress for a small strain with the use of the stress theorem [50].
136 Alternatively, the macroscopic stress can be also calculated using density functional
137 perturbation theory (DFPT) [51]. In this work, we have evaluated the elastic constants
138 of DC-HgGa₂S₄ as implemented in the VASP code: the ground state and fully relaxed
139 structures were strained in different directions according to their symmetry [52]. Total
140 energy variations have been evaluated according to a Taylor expansion for the total
141 energy with respect to the applied strain [53]. Due to this fact, it is important to check
142 that the strain used in the calculations guarantees the harmonic behavior. This procedure
143 allows the computation of the C_{ij} elastic constants in the Voigt notation where the
144 number of independent elastic constants is reduced by crystalline symmetry [54]. The
145 mechanical stability of the low-pressure phase of HgGa₂S₄ has been studied from a
146 theoretical point of view using the generalized stability criteria.

147

148 **4. Results and discussion**

149 **4.1. X-ray diffraction and structural properties**

150 As already commented, HgGa₂S₄ crystallizes in the tetragonal defect
151 chalcopyrite (DC) structure at room conditions [1-3]. **Table 1** shows the

152 crystallographic parameters of DC-HgGa₂S₄ at RP obtained from a Rietveld refinement
153 of XRD data taken from **Ref. [3]**. Results for our samples are comparable to our
154 theoretical calculations and to those of **Refs. 1 and 2** (see **Table 1**).

155 **Figure 1** shows the XRD patterns of HgGa₂S₄ from RP to 15.1 GPa taken with
156 the Xcalibur diffractometer. Those XRD patterns have been analyzed in the range $2\theta \leq$
157 18.3° due to the presence of intense peaks of the stainless-steel gasket at higher angles.
158 At the bottom of **Fig. 1** we show in solid line the measured XRD pattern of our sample
159 at RP along with the Miller indexes of the Bragg reflections for the DC phase. Vertical
160 marks representing the positions of the Bragg reflections are also plotted.
161 Diffractograms from RP to 15.1 GPa on upstroke could be indexed with the low-
162 pressure tetragonal DC phase. The diffraction peaks only move to higher angles as
163 pressure increases, thus indicating that compression causes a decrease of interplanar
164 distances. In the angular region $2\theta \leq 18.3^\circ$ the DC phase has nine Bragg peaks which
165 allow obtaining the pressure evolution of the unit-cell parameters by means of a Le Bail
166 refinement. Pressures, unit-cell parameters and volume for DC-HgGa₂Se₄ are listed in
167 **Table 2** along with the *R*-factors obtained from the Le Bail refinement. Broadening of
168 the diffraction peaks, caused by the deterioration of the quasi-hydrostatic conditions of
169 the experiment beyond 10 GPa, can be observed in **Fig. 1 [38, 55]**. In order to avoid the
170 effects of deviatoric stresses on the quantitative study of the structural properties of DC-
171 HgGa₂S₄, the axial compressibilities and the bulk modulus will be estimated using
172 experimental data below 10 GPa because in this range the methanol-ethanol mixture
173 maintains quasi-hydrostatic conditions **[38]**.

174 **Figure 2** shows the pressure dependence of the lattice parameters for DC-
175 HgGa₂S₄ from data obtained in XRD experiments (symbols) and from calculations
176 (solid line). The experimental axial compressibilities for *a* and *c* axes at RP, defined as

177 $\kappa_x = \frac{-1}{x} \frac{\partial x}{\partial P}$ and obtained by fitting of a Murnaghan EOS [56], are $\kappa_a = 7.6(6) \cdot 10^{-3}$
 178 GPa^{-1} and $\kappa_c = 5.3(8) \cdot 10^{-3} \text{GPa}^{-1}$. Our experiments show an anisotropy in the axial
 179 compression being the a axis more compressible than the c one. This result agrees with
 180 our theoretical results $\kappa_a = 8.9 \cdot 10^{-3} \text{GPa}^{-1}$ and $\kappa_c = 7.0 \cdot 10^{-3} \text{GPa}^{-1}$ and with previous
 181 results for other AB_2X_4 OVCs [18, 24, 26, 27, 32, 33].

182 **Figure 3** shows the pressure dependence of the volume of the DC phase in
 183 HgGa_2S_4 . EOS parameters of HgGa_2S_4 were determined by a least-squares fit of second
 184 order Birch-Murnaghan (BM2) and third-order Birch-Murnaghan (BM3) EOSs [57] to
 185 the experimental volume data. Weights derived from the experimental uncertainties in
 186 both pressure and volume were assigned to each data point in both fits. The fits were
 187 carried out with the v5.2 of the EoSFit software [58]. The RP values of the volume V_0
 188 and bulk modulus B_0 obtained from fitting experimental data below 10 GPa with a BM2
 189 EOS are summarized in **Table 3**. In the case of the BM2 EOS the first-pressure
 190 derivative of the bulk modulus B_0' is fixed to 4. The obtained value for the weighted
 191 chi-squared, χ^2_w , in the BM2 EOS fit is 1.16. The EOS parameters obtained with the
 192 BM3 EOS fit are included in **Table 3**. In this case, the refinement of the B_0' parameter
 193 does not improve the fit of the data because the χ^2_w increases to a value of 1.25 and the
 194 standard deviations of V_0 and B_0 increase with respect to those obtained with the BM2
 195 EOS, thus indicating that an expansion of the EOS to third order is not required to fit
 196 the data. These results show that the second-order equation of state is an adequate
 197 representation of the volume-pressure data of HgGa_2S_4 .

198 In order to obtain a direct indication of the compressional behavior of DC-
 199 HgGa_2S_4 and of the quality of the EOS fit, the P - V data are transformed into F - f data
 200 where F is the normalized stress and f the finite strain [58]. For the Birch-Murnaghan
 201 EOS, based upon the Eulerian definition of finite strain f_E , the normalized pressure is

202 defined as $F_E = P/(3f_E(1+2f_E)^{5/2})$ with the Eulerian strain defined as $f_E = [(V_0/V)^{2/3}-1]/2$
 203 [58]. In a F_E - f_E plot, if the data points all lie on a horizontal line of constant F_E then B_0'
 204 = 4, and the data can be fitted with a BM2. If the data lie on an inclined straight line, the
 205 slope is equal to $3B_0(B_0'-4)/2$, and the data will be adequately described by a BM3 [58].
 206 In both cases, the intercept on the vertical F_E axis is the value of B_0 . The F_E - f_E plot for
 207 DC-HgGa₂S₄ is shown in **Fig. 4** with the uncertainties in f_E and F_E . It is seen that a
 208 linear fit to experimental data (blue dashed line) gives a straight line almost parallel to
 209 the case when $B_0'=4$ (solid red line). A value of $B_0 = 48.5(7)$ GPa is obtained from the
 210 linear fit. The linear fit gives a small positive slope from which a $B_0' = 4.0(3)$ is
 211 obtained. These results show that the BM2 EOS is an adequate representation of the
 212 volume-pressure data of HgGa₂S₄ as has been previously found on the basis of
 213 statistical results from the EOS fits.

214 Theoretical data have been fitted with BM2 and BM3 EOSs and the results for
 215 the V_0 , B_0 and B_0' parameters are included in **Table 3**. It can be observed that our
 216 experimental and theoretical results are in relatively good agreement. For comparison
 217 purposes, **Table 4** summarizes the B_0 and B_0' parameters obtained experimentally for
 218 several AB_2X_4 OVCs. Since both parameters are strongly correlated [59] and they may
 219 depend on the hydrostatic conditions of the experiments [32], care should be taken
 220 when comparing B_0 values. For that reason the PTM used during the experiment is also
 221 reported in **Table 4**. It can be observed that for DC-HgGa₂S₄ the experimental B_0
 222 (48.4(3) GPa) obtained with the BM2 EOS is similar to that obtained in other OVCs.

223 Now we will study the evolution of the c/a ratio with pressure in DC-HgGa₂S₄
 224 since the tetragonal distortion, $\delta = 2 - c/a$, could give important information about the
 225 behavior of the sample on compression. Inset of **Fig. 3** shows the experimental
 226 (symbols) and theoretical (solid line) pressure dependence of the c/a ratio vs. pressure.

227 It can be observed that c/a increases with increasing pressure from 1.856 at RP to 1.929
228 at 15.1 GPa. Therefore, our results show that DC-HgGa₂S₄, like other DC compounds
229 [18, 24, 26, 27, 31-33], tends to a more symmetrical structure on compression.
230 Furthermore, the evolution of the experimental c/a ratio with pressure is also well
231 reproduced by our calculations. It must be noted that the increase of the c/a ratio has
232 been previously considered as a measure of cation-vacancy disorder [60, 61]. However,
233 since no cation-vacancy disorder is assumed in our calculations, the good agreement
234 between our experimental and theoretical results suggests that the tetragonal distortion
235 cannot be taken as a measure of the cation-vacancy disorder in the tetragonal DC
236 structure at any pressure as previously thought [15].

237 It was also thought that information on the cation-vacancy disorder could be
238 obtained from the study of the pressure dependence of the axial compressibilities κ_a and
239 κ_c and their difference [24, 33]. This information is shown for DC-HgGa₂S₄ in the top
240 and low panels of **Fig. 5** for XRD experiments and calculations, respectively. As can be
241 seen, in both cases, the κ_a and κ_c compressibilities decrease with pressure as observed
242 previously in other OVCs [24, 33]. Furthermore, the $\kappa_a - \kappa_c$ difference is positive at
243 every pressure, but has a non-linear pressure dependence with a positive pressure
244 coefficient at low pressures and a negative pressure coefficient at high pressures. The
245 value of the $\kappa_a - \kappa_c$ maximum for DC-HgGa₂S₄ is found at about 4 GPa. A similar
246 evolution was found previously for DC-MnGa₂Se₄ and HgGa₂Se₄ [24, 33]. In this
247 respect, it was proposed that the change in tendency of the difference $\kappa_a - \kappa_c$ with
248 pressure was a sign of the onset of the transformation from the DC phase to a disordered
249 structure (around 3 GPa in MnGa₂Se₄) [24]. This would imply that cation disorder is
250 increasing with pressure above that pressure. However, our calculations show a
251 maximum for $\kappa_a - \kappa_c$ at a similar pressure than in experiment despite cation disorder is

252 not considered in the calculations. Since we have obtained the same results now for DC-
253 HgGa_2S_4 than previously for DC- HgGa_2Se_4 [33], we reaffirm that unfortunately the
254 change of the pressure coefficient of $\kappa_a - \kappa_c$ cannot be considered a sign of the onset of
255 the cation disorder in the tetragonal DC structure of AB_2X_4 OVCs.

256 In order to understand better how the structure of DC- HgGa_2S_4 behaves under
257 compression we show in **Fig. 6 (a)** the theoretical pressure dependence of the cation-
258 anion and vacancy-anion distances in DC- HgGa_2S_4 . A good agreement is found
259 between the calculated and experimental distances at RP. The largest distance is that of
260 Hg-S, the intermediate distances are those of Ga(1)-S and Ga(2)-S, and the shortest
261 distance is that of vacancy-S. Hg-S, Ga(1)-S, and Ga(2)-S distances are much less
262 compressible than the vacancy-S distance, despite the latter is the smallest one. The
263 high compressibility of the vacancy-S distance is due to the weak repulsion between the
264 separated electron distributions of S atoms surrounding the vacancy. Consequently, S
265 atoms move towards the vacancy site at a faster rate than to the sites occupied by
266 cations. These calculated results for DC- HgGa_2S_4 agree nicely with those calculated for
267 DC- HgGa_2Se_4 [33] and with those experimentally obtained for DC- CdGa_2Se_4 from
268 XRD measurements [18]. For completeness, we show in **Fig. 6(b)** the compressibility of
269 the cation-anion and vacancy-anion internal distances for DC- HgGa_2S_4 as a function of
270 pressure. The distance compressibility decreases following the sequence “vacancy-S >
271 Hg-S > Ga(1)-S > Ga(2)-S”. At HP, the compressibility of all cation-anion distances
272 tends to approach to a similar value whilst the vacancy-S distance compressibility is still
273 much larger. The calculated compressibility at RP for the average Ga-S, Hg-S, and
274 vacancy-S distances are $2.7 \cdot 10^{-3} \text{ GPa}^{-1}$, $5.1 \cdot 10^{-3} \text{ GPa}^{-1}$, and $21.4 \cdot 10^{-3} \text{ GPa}^{-1}$;
275 respectively.

276

277 4.2. Elastic properties

278 DC-HgGa₂S₄ belongs to the tetragonal Laue group TII and has seven
279 independent second-order elastic constants named: C_{11} , C_{12} , C_{13} , C_{33} , C_{44} , C_{66} , and C_{16}
280 [33]. The formulas for the calculation of the elastic moduli with the use of the elastic
281 constants in the Laue group TII have not been derived analytically. This is due to the
282 presence of the off-diagonal shear elastic constant C_{16} which is usually different from
283 zero. However, it is possible to transform the seven components C_{ij} of the elastic tensor
284 of a TII crystal into the six components C'_{ij} of the elastic tensor of a TI crystal, for
285 which the formulas for the calculation of the elastic moduli are available. For that
286 purpose one needs to make C_{16} equal to zero by means of a rotation around the Z axis
287 through an angle given by [62, 63]:

$$288 \phi_{\kappa,\gamma} = \frac{1}{4} \arctan\left(\frac{4C_{16}}{C_{11} - C_{12} - 2C_{66}}\right) \quad (1)$$

289 Equation (1) gives two values for ϕ in the range $0 < \phi < |\pi/2|$ that correspond to
290 ϕ_{κ} and ϕ_{γ} where $\phi_{\gamma} = \phi_{\kappa} + \pi/4$ [63, 64]. For DC-HgGa₂S₄ at RP we obtain $\phi_{\kappa} = 3.72^\circ$ and
291 $\phi_{\gamma} = 48.72^\circ$.

292 The equations used to obtain the six independent C'_{ij} elastic constants of a TI
293 crystal as a function of the seven C_{ij} elastic constants of a TII crystal and the ϕ angle
294 have been taken from Ref. [64]. Table 5 shows the set of seven elastic constants C_{ij} at
295 RP obtained from our calculations together with the two sets of six C'_{ij} obtained for
296 angles ϕ_{κ} and ϕ_{γ} . The results for DC-HgGa₂S₄ are compared to the theoretical results for
297 DC-HgGa₂Se₄ [33], and for DC-CdGa₂S₄ and DC-CdGa₂Se₄ [65] (see Table 5). In
298 general, values for C_{ij} are similar in the four compounds but are slightly larger for

299 sulphides (CdGa_2S_4 and HgGa_2S_4) than for the corresponding selenides (CdGa_2Se_4 and
300 HgGa_2Se_4).

301 With the set of six C'_{ij} elastic constants for DC- HgGa_2S_4 , the bulk (B), and shear
302 (G) moduli for the tetragonal Laue group TI in the Reuss [66], Voigt [67], and Hill [68]
303 approximations, labeled with subscripts R , V , and H , respectively, have been calculated
304 by using the equations 2 to 7 given in Ref. [33] which were already used to calculate the
305 elastic moduli for DC- HgGa_2Se_4 (see Table 5). In the Reuss (Voigt) approximations,
306 uniform stress (strain) is assumed throughout the polycrystal [66, 67]. Hill has shown
307 that the Voigt and Reuss averages are limits and suggested that the actual effective B
308 and G elastic moduli can be approximated by the arithmetic mean of the two bounds
309 [68]. The Young (E) modulus and the Poisson's ratio (ν) are calculated by the equations
310 8 and 9 given in Ref. [33]. Table 5 summarizes the obtained values of B , G , E , and ν for
311 DC- HgGa_2S_4 at RP. It is found that DC- HgGa_2S_4 is more resistive to volume
312 compression than to shear ($B > G$). Note that we have obtained a value for the bulk
313 modulus in the Hill approximation of $B_H = 45.7$ GPa which is in very good agreement
314 with the value of $B_0 = 48.4(3)$ GPa obtained from our XRD measurements via a second
315 order Birch-Murnaghan EOS fit. This result gives us confidence about the correctness
316 of our elastic constants calculations.

317 With the values of the seven calculated C_{ij} at RP reported in Ref. 65 for Cd-
318 based compounds, we have obtained the six C'_{ij} at RP and the corresponding elastic
319 moduli for comparison with Hg-based compounds (see Table 5). We must note that for
320 DC- CdGa_2S_4 we obtain a value of the bulk modulus of 40.6 GPa instead of the value of
321 58.4 GPa reported by the authors.

322 Table 5 also includes the values of the ratio between the bulk and shear
323 modulus, B/G , and the shear anisotropy factor A . The B/G ratio is a simple relationship

324 given by Pugh [69], empirically linking the plastic properties of a material with its
 325 elastic moduli. According to the Pugh criterion a high B/G ratio is associated with
 326 ductility, whereas a low ratio corresponds to brittleness. The critical value for the B/G
 327 ratio is around 1.75, which separates ductile and brittle materials. In our particular case,
 328 we found a value of $B/G = 1.91$ in the Hill approximation indicating that the material
 329 should be ductile but close to the limit of ductility at RP. Therefore, experimental
 330 measurements are needed to determine the plastic behavior of HgGa_2S_4 in practice. The
 331 elastic anisotropy of crystals is of importance for both engineering science and crystal
 332 physics since it is highly correlated to the possibility of inducing microcracks in the
 333 materials [70]. This anisotropy is quantified in our DC sample with the shear anisotropy
 334 factor A that for our tetragonal cell is defined as $A=2C_{66}/(C_{11}-C_{12})$ [71]. If A is equal to
 335 1, no anisotropy exists. On the other hand, the more this parameter differs from 1, the
 336 more elastically anisotropic is the crystalline structure. In our particular case, $A = 1.96$
 337 and 0.51 for angles ϕ_x and ϕ_y , respectively. These values are rather different from 1 and
 338 evidence the anisotropy of our tetragonal cell at RP. Note that the anisotropy factors
 339 obtained for the two possible rotation angles follow the relation $0.51 = 1/1.96$, which is
 340 a direct consequence of the $\pi/4$ rotation around the z axis ($\phi_y = \phi_x + \pi/4$). We have
 341 also obtained the axial compressibilities κ_a and κ_c from our elastic constants
 342 calculations by using the equation 10 of Ref. [33]. **Table 5** includes the values for κ_a
 343 and κ_c obtained at RP which are in good agreement with those obtained experimentally.
 344 Again, this result gives us confidence about the correctness of our elastic constants
 345 calculations.

346 We have also obtained the values of the B/G ratio, A factor, and κ_a and κ_c axial
 347 compressibilities for DC- CdGa_2S_4 and DC- CdGa_2Se_4 which are included in **Table 5**.
 348 We have found that the κ_a and κ_c axial compressibilities for the two Cd-based

349 compounds obtained from C_{ij} data of **Ref. [65]** are not in good agreement with
350 experimental values for κ_a and κ_c . The experimental κ_a and κ_c for DC-CdGa₂S₄
351 estimated from **Ref [26]** are $\kappa_a = 5.9(8) \cdot 10^{-3} \text{ GPa}^{-1}$ and $\kappa_c = 4.5(7) \cdot 10^{-3} \text{ GPa}^{-1}$. For the
352 case of DC-CdGa₂Se₄, the experimental κ_a and κ_c estimated from **Ref [18]** are $\kappa_a =$
353 $12.5(9) \cdot 10^{-3} \text{ GPa}^{-1}$ and $\kappa_c = 8.3(6) \cdot 10^{-3} \text{ GPa}^{-1}$. The major discrepancy between
354 theoretical and experimental values for κ_a and κ_c in DC-CdGa₂Se₄ is that theoretical κ_c
355 has an unusual negative value of $-3.5 \cdot 10^{-3} \text{ GPa}^{-1}$ unlike the positive experimental one. In
356 the case of DC-CdGa₂S₄, the theoretical κ_a / κ_c ratio is smaller than 1, unlike the
357 experimental κ_a / κ_c ratio which shows that the a axis is more compressible than the c
358 one, as it is observed experimentally in all studied OVCs and in our calculations. These
359 discrepancies indicate that more accurate calculations for the elastic constants of DC-
360 CdGa₂S₄ and DC-CdGa₂Se₄ are needed.

361 In the following, we are going to study the mechanical stability of DC-HgGa₂S₄
362 at HP. For that purpose, we will analyze the pressure dependence of the elastic
363 constants. **Figure 7(a)** shows the evolution of the seven calculated C_{ij} of DC-HgGa₂S₄
364 with pressure which could be useful for comparison to future experimental
365 measurements of the elastic constants of DC-HgGa₂S₄ under pressure. It can be seen
366 that the C_{11} , C_{12} , C_{13} , C_{33} , and C_{66} elastic constants increase monotonically as pressure
367 increases. The C_{44} elastic constant increases up to a value of 9 GPa and above that
368 pressure it decreases as pressure increases. Finally, the C_{16} elastic constant remains
369 small in all the studied pressure range. In summary, the evolution of the seven C_{ij} with
370 pressure for HgGa₂S₄ is similar to that found in HgGa₂Se₄ **[33]**.

371 The study of the mechanical stability of a crystal under pressure requires the
372 generalization of the Born-Huang stability criteria to the case when an external load is
373 applied. In this way, the generalized stability criteria are obtained. For a detailed

374 explanation of how these generalized stability criteria are deduced, we refer the reader
 375 to Ref. [72]. In practice, these criteria for tetragonal crystals with six elastic constants
 376 are given by the following conditions [33, 72]:

$$377 \quad C_{11} - P > 0, \quad (2)$$

$$378 \quad C_{44} - P > 0, \quad (3)$$

$$379 \quad C_{66} - P > 0, \quad (4)$$

$$380 \quad C_{11} - C_{12} - 2P > 0 \quad (5)$$

$$381 \quad (C_{33} - P)(C_{11} + C_{12}) - 2(C_{13} + P)^2 > 0 \quad (6)$$

382

383 All the above criteria are satisfied for DC-HgGa₂S₄ at RP, thus this tetragonal
 384 crystal is mechanically stable at RP, as expected. **Figure 7(b)** shows the pressure
 385 dependence of the six elastic constants for the case of $\phi_\kappa = 3.72^\circ$ in order check whether
 386 DC-HgGa₂S₄ satisfies **Eqs. (2) to (6)** at HP. It can be observed that **Eq. (6)** is violated at
 387 a pressure of 13.8 GPa, **Eq. (3)** is violated at a pressure of 22.1 GPa, and **Eq. (5)** is
 388 violated at a pressure of 25.3 GPa. We highlight the fact that the pressures at which
 389 **Eqs. (6), (3) and (5)** are not satisfied are the same for both ϕ_κ and ϕ_γ transformations.
 390 Therefore, the study of the mechanical stability of DC-HgGa₂S₄ suggests that the
 391 tetragonal phase becomes mechanically unstable above a pressure of 13.8 GPa. This
 392 pressure is consistent with the pressure at which dark linear defects are observed. These
 393 defects are precursors of a phase transition of DC-HgGa₂S₄ to a disordered structure
 394 above 18 GPa and to a Raman-inactive phase above 23 GPa [34].

395 To conclude, we report in **Fig. 8** and discuss the pressure dependence of the B ,
 396 G and E elastic moduli, the ν Poisson's ratio, the B/G ratio and the A factor. It can be
 397 observed that the bulk modulus increases as pressure increases reaching a value of $B_H =$

398 93.9 GPa at 14 GPa. The shear modulus increases with pressure reaching a maximum
399 value of $G_H = 29.3$ GPa at 14.6 GPa and above that pressure it decreases as pressure
400 increases. In the case of the Young modulus it increases with pressure reaching a
401 maximum value of $E_H = 80.0$ GPa at 15.7 GPa and above that pressure it decreases as
402 pressure increases. The Poisson's ratio and the B/G ratio increase as pressure increases
403 reaching a value $\nu_H = 0.36$ and $B_H/G_H = 3.19$ at 14 GPa. In the case of the shear
404 anisotropy factor A it is found that for $\phi_\kappa = 3.72^\circ$, A decreases reaching a minimum
405 value 1.68 at 10.7 GPa and above that pressure it increases with pressure reaching a
406 value of 1.83 at 20 GPa. In this respect, we want to stress that the change of the pressure
407 coefficient of the theoretically calculated G and E elastic moduli at HP seems to be
408 related to the mechanical instability of the DC structure above 13.8 GPa. A similar
409 result was found for HgGa_2Se_4 [33]. Therefore, these behaviors could be related to the
410 onset of the cation-vacancy disorder process and evidenced by the appearing of dark
411 linear defects visually observed in HP measurements as already commented, thus
412 suggesting that the appearance of dark linear defects could be related to the mechanical
413 instability. In this respect, more experimental and theoretical work is needed to confirm
414 whether this fact is a general trend in other DC compounds and in general in adamantine
415 OVCs.

416

417 **5. Conclusions**

418 We have performed XRD measurements at room temperature in defect
419 chalcopyrite HgGa_2S_4 at high pressures and have compared the results with *ab initio*
420 total energy calculations. Experiments show that the pressure dependence of the
421 volume, lattice parameters, and axial ratio of DC- HgGa_2S_4 is similar to that of other

422 AGa_2X_4 ($A=Mn, Zn, Cd, Hg; X=S, Se$) adamantine OVCs. The evolution with pressure
423 of the internal cation-anion and vacancy-anion distances is given showing that the
424 vacancy-S distance is the most compressible one.

425 Additionally, a theoretical study of the elastic properties of DC-HgGa₂S₄ at
426 different pressures has been accomplished. At RP the elastic constants and elastic
427 moduli obtained for the tetragonal phase are in agreement with other calculations for
428 similar compounds of the AGa_2X_4 family. From those results it can be observed that the
429 elastic moduli of sulphides are slightly larger than those of the corresponding selenides.
430 Furthermore, the evolution of the elastic constants with pressure has been reported for
431 future comparison with experimental measurements. From those results we have
432 performed a study of the mechanical stability of the tetragonal phase at high pressures
433 and found that the tetragonal DC-HgGa₂S₄ crystal becomes mechanically unstable at
434 pressures above 13.8 GPa.

435

436 **Acknowledgements**

437 This study was supported by the Spanish government MEC under Grants No:
438 MAT2010-21270-C04-01/03/04 and CTQ2009-14596-C02-01, by the Comunidad de
439 Madrid and European Social Fund (S2009/PPQ-1551 4161893), by MALTA Consolider
440 Ingenio 2010 project (CSD2007-00045), by Generalitat Valenciana (GVA-ACOMP-
441 2013-1012), and by the Vicerrectorado de Investigación y Desarrollo of the Universidad
442 Politécnica de Valencia (UPV2011-0914 PAID-05-11 and UPV2011-0966 PAID-06-
443 11). E.P-G., A.M., and P.R-H. acknowledge computing time provided by Red Española
444 de Supercomputación (RES) and MALTA-Cluster. J. A. S. acknowledges Juan de la
445 Cierva fellowship program for financial support.

446 **References**

- 447 [1] H. Hahn, G. Frank, W. Klinger, A. Störger, G. Störger, *Z. Anorg. Allg. Chem.* 279
448 (1955) 241.
- 449 [2] H. Schwer, V. Krämer, *Z Kristallogr.* 190 (1990) 103.
- 450 [3] V.V. Atuchin, V.G. Kesler, V.V. Ursaki, and V.E. Tezlevan, *Solid State Commun.*
451 138 (2006) 250.
- 452 [4] A. MacKinnon, in *Tables of Numerical Data and Functional Relationships in*
453 *Science and Technology*, edited by O. Madelung, M. Schulz, and H. Weiss, Landolt-
454 Börnstein New Series, Group III, Vol. 17, pt. h, Springer-Verlag, Berlin, 1985, p. 124.
- 455 [5] A.N. Georgobiani, S.I. Radautsan, and I. M. Tiginyanu, *Sov. Phys. Semicond.* 19
456 (1985) 121.
- 457 [6] J.E. Bernard and A. Zunger, *Phys. Rev. B* 37 (1988) 6835.
- 458 [7] X. Jiang and W.R.L. Lambrecht, *Phys. Rev. B* 69 (2004) 035201.
- 459 [8] B.F. Levine, C.G. Bethea, H.M. Kasper, F.A. Thiel, *IEEE J. Quantum Electron.* QE-
460 12 (1976) 367.
- 461 [9] V.V. Ursaki, P.C. Ricci, I. Tiginyanu, A. Anedda, N.N. Syrbu, V.E. Tezlevan, *J.*
462 *Phys. Chem. Solids* 63 (2002) 1823.
- 463 [10] F. Rotermund and V. Petrov, *Optics Letters* 25 (2000) 746.
- 464 [11] V. V. Badikov, N. V. Kuzmin, V. B. Laptev, A. L. Malinovsky, K. V. Mitin, G. S.
465 Nazarov, E. A. Ryabov, A. M. Seryogin, and N. I. Shchebetova, *Quantum Electron.* 34
466 (2004) 451.

- 467 [12] F. Rotermund, V. Petrov, and F. Noack, *Opt. Commun.* 185 (2000) 177.
- 468 [13] I. I. Burlakov, Y. Raptis, V. V. Ursaki, E. Anastassakis, and I. M. Tiginyanu, *Solid*
469 *State Commun.* 101 (1997) 377.
- 470 [14] J. González, R. Rico, E. Calderón, M. Quintero, and M. Morocoima, *phys. stat. sol.*
471 (b) 211 (1999) 45.
- 472 [15] V.V. Ursaki, I.I. Burlakov, I.M. Tiginyanu, Y.S. Raptis, E. Anastassakis, and A.
473 Anedda, *Phys. Rev. B* 59 (1999) 257.
- 474 [16] M. Fuentes-Cabrera and O.F. Sankey, *J. Phys.: Condens. Matter* 13 (2001) 1669.
- 475 [17] M. Fuentes-Cabrera, *J. Phys.: Condens. Matter* 13 (2001) 10117.
- 476 [18] A. Grzechnik, V.V. Ursaki, K. Syassen, I. Loa, I.M. Tiginyanu, and M. Handfland,
477 *J. Solid State Chem.* 160 (2001) 205.
- 478 [19] T. Mitani, S. Onari, K. Allakhverdiev, F. Gashimzade, and T. Kerimova, *phys. stat.*
479 *sol. (b)* 223 (2001) 287.
- 480 [20] A. Tatsi, D. Lampakis, E. Liarokapis, S.A. López, L. Martínez, and W. Giriat, *High*
481 *Press. Res.* 22 (2002) 89.
- 482 [21] I. M. Tiginyanu, V.V. Ursaki, F.J. Manjón, and V.E. Tezlevan, *J. Phys. Chem.*
483 *Solids* 64 (2003) 1603.
- 484 [22] T. Mitani, T. Naitou, K. Matsuishi, S. Onari, K. Allakhverdiev, F. Gashimzade, and
485 T. Kerimova, *phys. stat. sol. (b)* 235 (2003) 321.
- 486 [23] K. Allakhverdiev, F. Gashimzade, T. Kerimova, T. Mitani, T. Naitou, K.
487 Matsuishi, and S. Onari, *J. Phys. Chem. Solids* 64 (2003) 1597.

488 [24] J. Marquina, Ch. Power, P. Grima, M. Morocoima, M. Quintero, B. couzinet, J.C.
489 Chervin, P. Munsch, and J. González, J. Appl. Phys. 100 (2006) 093513.

490 [25] S. Meenakshi, V. Vijyakumar, B.K. Godwal, A. Eifler, I. Orgzall, S. Tkachev, and
491 H.D. Hochheimer, J. Phys. Chem. Solids 67 (2006) 1660.

492 [26] D. Errandonea, R.S. Kumar, F.J. Manjón, V.V. Ursaki, and I.M. Tiginyanu, J.
493 Appl. Phys. 104 (2008) 063524.

494 [27] S. Meenakshi, V. Vijyakumar, A. Eifler, and H.D. Hochheimer, J. Phys. Chem.
495 Solids 71 (2010) 832.

496 [28] P. Singh, M. Sharma, U.P. Verma, and P. Jensen, Z. Kristallogr. 225 (2010) 508.

497 [29] F.J. Manjón, O. Gomis, P. Rodríguez-Hernández, E. Pérez-González, A. Muñoz,
498 D. Errandonea, J. Ruiz-Fuertes, A. Segura, M. Fuentes-Cabrera, I. Tiginyanu, and V.V.
499 Ursaki, Phys. Rev. B 81 (2010) 195201.

500 [30] U. P. Verma, P. Singh, and P. Jensen, phys. status solidi (b) 248 (2011) 1682.

501 [31] O. Gomis, R. Vilaplana, F. J. Manjón, E. Pérez-González, J. López-Solano, P.
502 Rodríguez-Hernández, A. Muñoz, D. Errandonea, J. Ruiz-Fuertes, A. Segura, D.
503 Santamaría-Pérez, I. M. Tiginyanu, and V.V. Ursaki, J. Appl. Phys. 111 (2012)
504 013518.

505 [32] O. Gomis, R. Vilaplana, F.J. Manjón, D. Santamaría-Pérez, D. Errandonea, E.
506 Pérez-González, J. López-Solano, P. Rodríguez-Hernández, A. Muñoz, I. M. Tiginyanu,
507 and V. V. Ursaki, Mat. Res. Bull. 48 (2013) 2128.

- 508 [33] O. Gomis, R. Vilaplana, F.J. Manjón, D. Santamaría-Pérez, D. Errandonea, E.
509 Pérez-González, J. López-Solano, P. Rodríguez-Hernández, A. Muñoz, I. M. Tiginyanu,
510 and V. V. Ursaki, *J. Appl. Phys.* 113 (2013) 073510.
- 511 [34] R. Vilaplana, M. Robledillo, O. Gomis, J. A. Sans, F.J. Manjón, E. Pérez-
512 González, P. Rodríguez-Hernández, A. Muñoz, I. M. Tiginyanu, and V. V. Ursaki, *J.*
513 *Appl. Phys.* 113 (2013) 093512.
- 514 [35] I.M. Tiginyanu, N. A. Modovyan, and O. D. Stoika, *Fiz. Tverd. Tela* 34 (1992)
515 967; *idem*, *Sov. Phys. Solid State* 43 (1992) 527.
- 516 [36] D. Santamaría-Pérez, A. Vegas, C. Muehle, and M. Jansen, *Acta Cryst. B* 67
517 (2011) 109.
- 518 [37] D. Santamaría-Pérez, M. Marqués, R. Chuliá-Jordán, J. M. Menéndez, O. Gomis, J.
519 Ruiz-Fuertes, J. A. Sans, D. Errandonea, and J. M. Recio, *Inorg. Chem.* 51 (2012) 5289.
- 520 [38] S. Klotz, J. C. Chervin, P. Munsch, and G. Le Marchand, *J. Phys. D: Appl. Phys.*
521 42 (2009) 075413.
- 522 [39] D. Errandonea, Y. Meng, M. Somayazulu, D. Häusermann, *Physica B* 355 (2005)
523 116.
- 524 [40] H. K. Mao, J. Xu, and P. M. Bell, *J. Geophys. Res.* 91 (1986) 4673.
- 525 [41] D. Errandonea, R. Boehler, S. Japel, M. Mezouar, and L.R. Benedetti, *Phys. Rev. B*
526 73 (2006) 092106.
- 527 [42] Oxford Diffraction (2006). *CrysAlis*. Oxford Diffraction Ltd, Abingdon, England.
- 528 [43] J. Laugier and B. Bochu, <http://www.ccp14.ac.uk/tutorial/lmgp/>

- 529 [44] W. Kraus and G. Nolze, *J. Appl. Crystallogr.* 29 (1996) 301.
- 530 [45] A. C. Larson and R. B. von Dreele, LANL Report 86-748 (2004).
- 531 [46] B. H. Toby, *J. Appl. Cryst.* 34 (2001) 210.
- 532 [47] G. Kresse and J. Hafner, *Phys. Rev. B* 47 (1993) 558; 49 (1994) 14251; G. Kresse,
533 and J. Furthmüller, *Comput. Mater. Sci.* 6 (1996) 15; *Phys. Rev. B* 54 (1996) 11169.
- 534 [48] J. P. Perdew, A. Ruzsinszky, G. I. Csonka, O. A. Vydrov, G. E. Scuseria, L. A.
535 Constantin, X. Zhou, and K. Burke, *Phys. Rev. Lett.* 100 (2008) 136406.
- 536 [49] A. Mujica, A. Rubio, A. Muñoz, R. J. Needs, *Rev. Mod. Phys.* 75 (2003) 863.
- 537 [50] N. Chetty, A. Muñoz, and R. M. Martin, *Phys. Rev. B* 40 (1989) 11934.
- 538 [51] S. Baroni, S. de Gironcoli, A. Dal Corso, and P. Giannozzi, *Rev. Mod. Phys.* 73
539 (2001) 515.
- 540 [52] Y. Le Page and P. Saxe, *Phys. Rev. B* 65 (2002) 104104.
- 541 [53] O. Beckstein, J. E. Klepeis, G. L. W. Hart, and O. Pankratov, *Phys. Rev. B* 63
542 (2001) 134112.
- 543 [54] J. F. Nye, *Physical properties of crystals. Their representation by tensor and*
544 *matrices*, Oxford University Press, 1957.
- 545 [55] E. Bandiello, D. Errandonea, D. Martinez-Garcia, D. Santamaria-Perez, and F. J.
546 Manjon, *Phys. Rev. B* 85 (2012) 024108.
- 547 [56] M. D. Frogley, J. L. Sly, and D. J. Dunstan, *Phys. Rev. B* 58 (1998) 12579.
- 548 [57] F. Birch, *J. Geophys. Res.* 83 (1978) 1257.

- 549 [58] R. J. Angel, Equations of state, in: R. M. Hazen, R. T. Downs (Eds.), High-
550 pressure and high-temperature crystal chemistry. MSA Reviews in Mineralogy and
551 Geochemistry 41, 2000, pp. 35–60.
- 552 [59] R. J. Angel, J. L. Mosenfelder, and C. S. J. Shaw, Phys. Earth Planet. Inter. 124
553 (2001) 71.
- 554 [60] L. Garbato, F. Ledda, and A. Rucci, Prog. Cryst. Growth Charact. 15 (1987) 1.
- 555 [61] L. Gastaldi, M.G. Simeone, and S. Viticoli, Solid State Commun. 55 (1985) 605.
- 556 [62] A. G. Khatkevich, Sov. Phys. Crystallogr. 6 (1962) 561.
- 557 [63] J. M. Farley, G. A. Saunders, and D. Y. Chung, J. Phys. C: Solid State Phys. 6
558 (1973) 2010.
- 559 [64] J. M. Farley, and G. A. Saunders, J. Phys. C: Solid State Phys. 5 (1972) 3021.
- 560 [65] S.-H. Ma, Z.-Y. Jiao, X.-Z. Zhang, J. Mater. Sci. 47 (2012) 3849.
- 561 [66] A. Reuss, and Z. Angew, Math. Mech. 9 (1929) 49.
- 562 [67] W. Voigt, Lehrbuch der Kristallphysik, Teubner, Leipzig, 1928.
- 563 [68] R. Hill, Proc. Phys. Soc. London, A 65 (1952) 349.
- 564 [69] S. F. Pugh, Philos. Mag. 45 (1954) 823.
- 565 [70] V. Tvergaard, and J. W. Hutchinson, J. Am. Ceram. Soc. 71 (1988) 157.
- 566 [71] K. Lau, and A. K. McCurdy, Phys. Rev. B 58 (1998) 8980.
- 567 [72] G. Grimvall, B. Magyari-Köpe, V. Ozolinš, and K. A. Persson, Rev. Mod. Phys. 84
568 (2012) 945.

570 **Table 1.** Experimental and theoretically calculated lattice parameters and relative
 571 atomic positions of tetragonal DC-HgGa₂S₄ at RP. The Rietveld refinement carried out
 572 at RP has residuals R_p = 16.5 %, and R_{wp} = 9.7 %. Hg, Ga(1), Ga(2), and the vacancy
 573 are located at the 2*a* (0,0,0), 2*b* (0,0,0.5), 2*c* (0,0.5,0.25), and 2*d* (0,0.5,0.75) Wyckoff
 574 positions, respectively. The relative atomic coordinates of the sulfur anion located at the
 575 8*g* (*x,y,z*) Wyckoff position are given in the table.

576

	X-ray diffraction ^a	<i>Ab initio</i> PBEsol ^b	X-ray diffraction ^c	X-ray diffraction ^d
<i>a</i> (Å)	5.5095(3)	5.5125	5.507	5.5106(1)
<i>c</i> (Å)	10.2308(6)	10.2015	10.23	10.2392(2)
S site: 8 <i>g</i>	x= 0.272(1) y = 0.268(1) z=0.1375(6)	x= 0.2743 y=0.2665 z =0.1390	x = 0.275 y = 0.265 z = 0.139	x =0.2718(3) y = 0.2675(3) z =0.1374(1)

577

578

^a Obtained from experimental results of Ref. [3].

579

^b Our calculations.

580

^c Ref. 1.

581

^d Ref. 2.

582

583

584

585 **Table 2.** Experimental pressure (P), unit-cell parameters (a , c) and volume (V) of DC-
586 HgGa_2S_4 with their standard deviations. The R_p and R_{wp} factors obtained from a Von
587 Dreele-type Le Bail refinement are also given.

P GPa	Esd (P) GPa	a Å	esd (a) Å	c Å	esd (c) Å	V Å ³	esd (V) Å ³	R_p (%)	R_{wp} (%)
0.00	0.00	5.506	0.001	10.219	0.003	309.80	0.21	7.6	18.1
0.03	0.01	5.505	0.001	10.217	0.003	309.61	0.20	7.2	18.2
0.68	0.01	5.477	0.001	10.186	0.003	305.52	0.20	11.9	18.4
1.20	0.01	5.460	0.001	10.162	0.002	302.90	0.17	8.2	17.4
1.35	0.01	5.449	0.001	10.157	0.002	301.57	0.17	8.0	17.4
2.04	0.01	5.425	0.001	10.128	0.002	298.01	0.17	7.7	16.9
2.20	0.01	5.422	0.001	10.114	0.004	297.30	0.23	9.7	16.4
2.75	0.01	5.400	0.001	10.096	0.002	294.39	0.17	7.5	17.9
3.73	0.01	5.364	0.001	10.048	0.002	289.13	0.17	7.1	17.0
3.95	0.01	5.359	0.001	10.052	0.002	288.68	0.17	8.0	17.4
4.67	0.01	5.339	0.001	10.021	0.002	285.67	0.16	7.8	18.1
5.30	0.01	5.318	0.001	9.999	0.002	282.73	0.16	8.5	18.6
5.74	0.01	5.311	0.001	9.990	0.003	281.83	0.19	10.5	18.1
6.05	0.01	5.297	0.001	9.975	0.002	279.85	0.16	6.1	15.8
6.62	0.01	5.278	0.001	9.962	0.002	277.48	0.16	8.8	18.1
6.80	0.01	5.276	0.001	9.958	0.003	277.15	0.19	12.7	20.0
7.30	0.01	5.257	0.001	9.948	0.002	274.94	0.16	8.0	17.5
8.20	0.01	5.238	0.001	9.920	0.003	272.13	0.19	11.6	17.8
11.00	0.02	5.168	0.001	9.878	0.004	263.86	0.21	10.8	17.9
13.30	0.02	5.129	0.001	9.840	0.004	258.82	0.21	10.6	18.8
15.10	0.02	5.089	0.001	9.818	0.005	254.24	0.23	11.7	20.5

588

589 **Table 3.** Experimentally determined and calculated EOS for DC-HgGa₂S₄ at RP. Last
 590 column indicates the EOS type used (BM2 = Birch-Murnaghan of order 2, BM3 =
 591 Birch-Murnaghan of order 3).

592

	V_0 (Å ³)	B_0 (GPa)	B_0'	EOS type
Experiment	309.77(11)	48.4(3)	4 (fixed)	BM2
Experiment	309.80(14)	48.1(9)	4.1(3)	BM3
Calculation	309.8(2)	44.0(4)	4 (fixed)	BM2
Calculation	310.4(1)	40.8(1)	4.9(1)	BM3

593

594

595

596 **Table 4.** Experimental bulk modulus (B_0), and its pressure derivative (B_0') at RP for
597 several OVCs. The case when the B_0' parameter was fixed to 4 in the EOS fit is
598 indicated. The PTM used in the different experiments is also included. Last column
599 indicates the EOS type used (M = Murnaghan, BM2 = Birch-Murnaghan of order 2,
600 BM3 = Birch-Murnaghan of order 3).

Compound	B_0 (GPa)	B_0'	PTM	Reference	EOS type
CdAl ₂ S ₄	44.6(1)	4 (fixed)	methanol-ethanol	27	BM2
CdAl ₂ Se ₄	52.1	4 (fixed)	methanol-ethanol	25	BM2
CdGa ₂ S ₄	64(2)	4.1(3)	silicone oil	26	BM3
CdGa ₂ Se ₄	41.5(2)	5(1)	methanol-ethanol	18	M
HgAl ₂ Se ₄	66(1.5)	4 (fixed)	paraffin oil	27	BM2
HgGa ₂ S ₄	48.4(3)	4 (fixed)	methanol-ethanol	This work	BM2
	48.1(9)	4.1(3)			BM3
HgGa ₂ Se ₄	53(9)	6(2)	MgO	32	BM3
	39(2)	5.2(4)	methanol-ethanol	33	BM3
MnGa ₂ Se ₄	44(2) ^a	3.8(4) ^a	methanol-ethanol, neon, and silicone oil	24	M
ZnGa ₂ Se ₄	47(2)	3.9(3)	silicone oil	26	BM3

601

602 ^a B_0 and B_0' parameters were obtained in **Ref. 24** by means of a single EOS fit to data
603 from three different experiments using each one of the three PTM indicated in the table.

604 **Table 5.** Seven C_{ij} and six C'_{ij} ($C'_{16} = 0$) calculated elastic constants (in GPa) for DC-
605 HgGa_2S_4 at RP. The elastic moduli B , G , and E (in GPa) and Possion's ratio (ν) are
606 given in the Voigt, Reuss and Hill approximations, labeled respectively with subscripts
607 V , R , and H . The B/G ratio and the shear anisotropy factor (A) are also included. The
608 axial compressibilities κ_a and κ_c obtained from the elastic constants calculations are also
609 given. Calculated data for DC- HgGa_2Se_4 [33], DC- CdGa_2Se_4 and DC- CdGa_2S_4 are also
610 added [65] for comparison.

611

	DC- HgGa_2S_4	DC- HgGa_2Se_4	DC- CdGa_2S_4	DC- CdGa_2Se_4
C_{11}	65.6 ^a	54.2 ^b	61.8 ^c	52.5 ^c
C_{12}	32.5 ^a	24.3 ^b	24.7 ^c	20.4 ^c
C_{13}	38.0 ^a	31.2 ^b	35.7 ^c	38.8 ^c
C_{33}	63.4 ^a	55.5 ^b	50.0 ^c	60.0 ^c
C_{44}	35.6 ^a	29.9 ^b	33.9 ^c	31.6 ^c
C_{66}	31.6 ^a	26.2 ^b	27.0 ^c	16.0 ^c
C'_{16}	-2.0 ^a	-0.3 ^b	-2.7 ^c	-1.9 ^c
C'_{11}	65.3 ^d , 80.9 ^e	54.2 ^f , 65.5 ^g	61.0 ^{h,i} , 71.0 ^{h,j}	50.6 ^{h,k} , 54.3 ^{h,l}
C'_{12}	32.8 ^d , 17.2 ^e	24.3 ^f , 13.0 ^g	25.5 ^{h,i} , 15.4 ^{h,j}	22.3 ^{h,k} , 18.6 ^{h,l}
C'_{13}	38.0 ^d , 38.0 ^e	31.2 ^f , 31.2 ^g	35.7 ^{h,i} , 35.7 ^{h,j}	38.8 ^{h,k} , 38.8 ^{h,l}
C'_{33}	63.4 ^d , 63.4 ^e	55.5 ^f , 55.5 ^g	50.0 ^{h,i} , 50.0 ^{h,j}	60.0 ^{h,k} , 60.0 ^{h,l}
C'_{44}	35.6 ^d , 35.6 ^e	29.9 ^f , 29.9 ^g	33.9 ^{h,i} , 33.9 ^{h,j}	31.6 ^{h,k} , 31.6 ^{h,l}
C'_{66}	31.9 ^d , 16.3 ^e	26.2 ^f , 14.9 ^g	27.8 ^{h,i} , 17.7 ^{h,j}	17.9 ^{h,k} , 14.1 ^{h,l}
B_V, B_R, B_H	45.7, 45.7, 45.7	37.5, 37.2, 37.4	58.4 ^c 40.6 ^h , 40.6 ^h , 40.6 ^h	36.1 ^c 40.1 ^h , 36.1 ^h , 38.1 ^h
G_V, G_R, G_H	26.3, 21.6, 24.0	22.3, 18.8, 20.6	24.1 ^h , 17.3 ^h , 20.7 ^h	20.3 ^h , 13.6 ^h , 16.9 ^h
E_V, E_R, E_H	66.2, 56.0, 61.2	55.9, 48.4, 52.2	60.4 ^h , 45.5 ^h , 53.1 ^h	52.1 ^h , 36.3 ^h , 44.3 ^h
ν_V, ν_R, ν_H	0.26, 0.30, 0.28	0.25, 0.28, 0.27	0.25 ^h , 0.31 ^h , 0.28 ^h	0.28 ^h , 0.33 ^h , 0.31 ^h
$B_V/G_V, B_R/G_R, B_H/G_H$	1.74, 2.11, 1.91	1.68, 1.98, 1.81	1.68 ^h , 2.35 ^h , 1.96 ^h	1.98 ^h , 2.66 ^h , 2.25 ^h
A	1.96 ^d , 0.51 ^e	1.75 ^f , 0.57 ^g	1.57 ^{h,i} , 0.64 ^{h,j}	1.27 ^{h,k} , 0.79 ^{h,l}
κ_a, κ_c (10^{-3} GPa^{-1})	7.6, 6.6	10.1, 6.7	8.1 ^h , 8.5 ^h	15.6 ^h , -3.5 ^h

612

613 ^a Our calculations.

614 ^b Data taken from **Ref. [33]**.

615 ^c Data taken from **Ref. [65]**.

616 ^{d,e} Rotation angle of $\phi_x = 3.72^\circ$ and $\phi_y = 48.72^\circ$, respectively.

617 ^{f,g} Rotation angle of $\phi_x = 0.76^\circ$ and $\phi_y = 45.76^\circ$, respectively.

618 ^h Obtained after the elastic constants reported in **Ref. [65]**.

619 ^{i,j} Rotation angle of $\phi_\kappa = 8.20^\circ$ and $\phi_\gamma = 53.20^\circ$, respectively.

620 ^{k,l} Rotation angle of $\phi_\kappa = 22.27^\circ$ and $\phi_\gamma = 67.27^\circ$, respectively.

621

622

623 **Figure captions**

624

625 **Figure 1.** Room temperature XRD patterns of HgGa₂S₄ at different pressures from RP
626 up to 15.1 GPa. In all diagrams, the background was subtracted. In the XRD pattern at
627 RP, Bragg reflections are indicated with vertical ticks.

628 **Figure 2.** Lattice parameters of the DC phase of HgGa₂S₄ as a function of pressure.
629 Symbols refer to experimental data. Theoretical results are plotted with solid line.

630 **Figure 3. (Color online)** Volume of the DC phase of HgGa₂S₄ as a function of
631 pressure. Experimental data (symbols) and their fit with a BM2 (red dashed line) and a
632 BM3 (blue dotted line) EOS are shown. The fit with a BM2 and BM3 EOS to
633 theoretical data is shown with solid and dash-dotted lines, respectively. The inset shows
634 the evolution of the c/a ratio of the DC phase as a function of pressure: experimental
635 data (symbols), theoretical data (solid line).

636 **Figure 4.** Volume-pressure data of DC-HgGa₂S₄ displayed as a plot of the normalized
637 pressure F_E against the Eulerian strain f_E . The blue dashed line is a linear fit to
638 experimental $F_E - f_E$ data. Solid red line represents the case of a BM2 EOS with $B_0' = 4$.

639 **Figure 5. (Color online)** Left side of panel: κ_a and κ_c vs. pressure. Right side of panel:
640 $(\kappa_a - \kappa_c)$ vs. pressure. Results correspond to: (a) XRD experiments, (b) PBEsol
641 calculations.

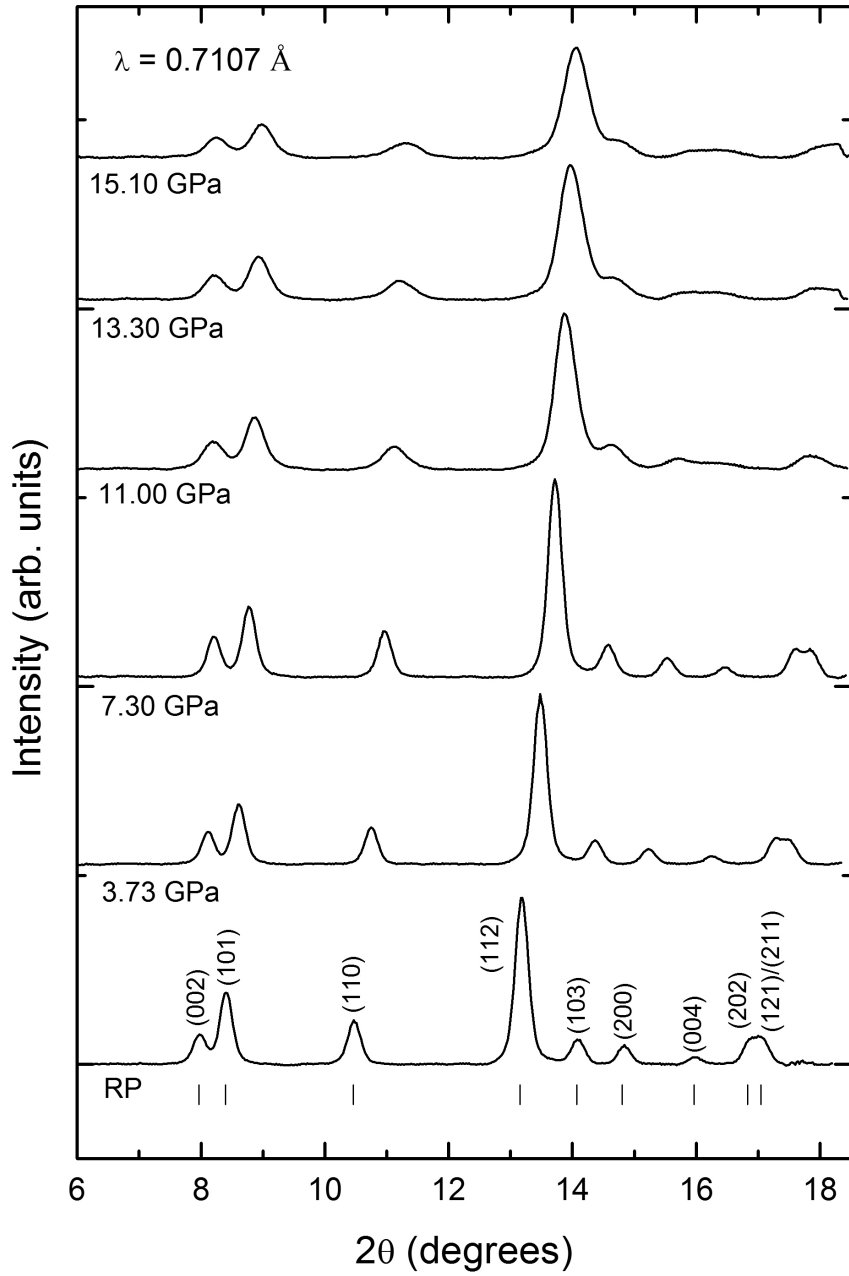
642 **Figure 6. (Color online)** (a) Calculated cation-anion and vacancy-anion distances, and
643 (b) distance compressibilities as a function of pressure for DC-HgGa₂S₄.

644 **Figure 7. (Color online)** Pressure dependence of the theoretical elastic constants of
645 DC-HgGa₂S₄: (a) Seven C_{ij} elastic constants and (b) Six C'_{ij} elastic constants. Solid
646 lines connecting the calculated data points are guides to the eyes.

647

648 **Figure 8. (Color online)** Pressure dependence of (a) B , (b) G , (c) E , (d) ν , (e) B/G , and
649 (f) A . Squares, circles, and triangles refer to the Voigt, Reuss, and Hill approximations;
650 respectively. Data for the A anisotropy factor are shown for $\phi_\kappa = 3.72^\circ$. Solid lines
651 connecting the calculated data points are guides to the eyes in panels (a) to (e). Solid
652 line in panel (f) represents the behavior of A with pressure.

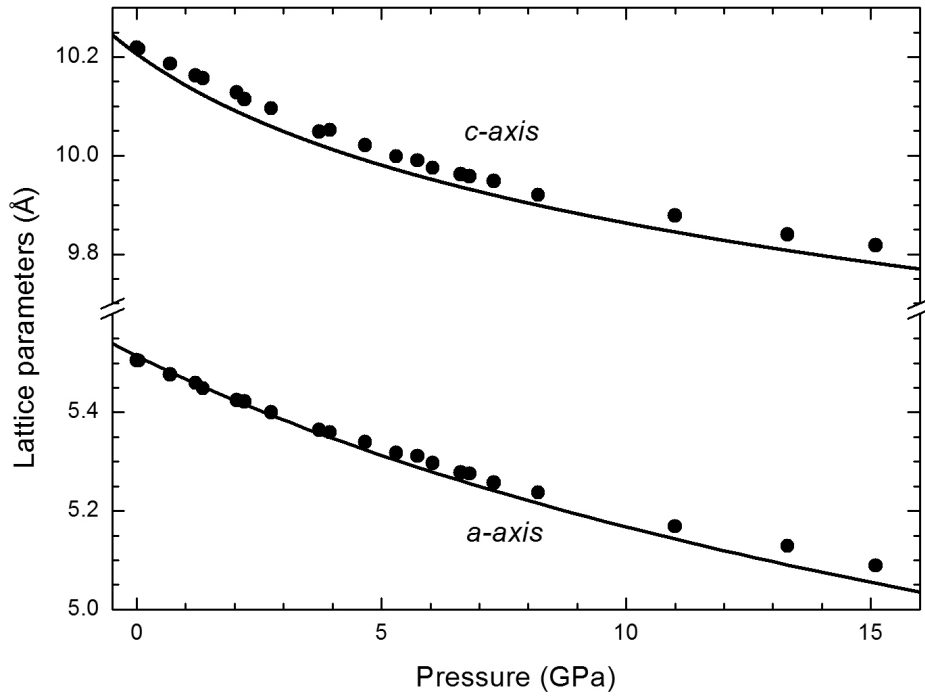
653



655

656

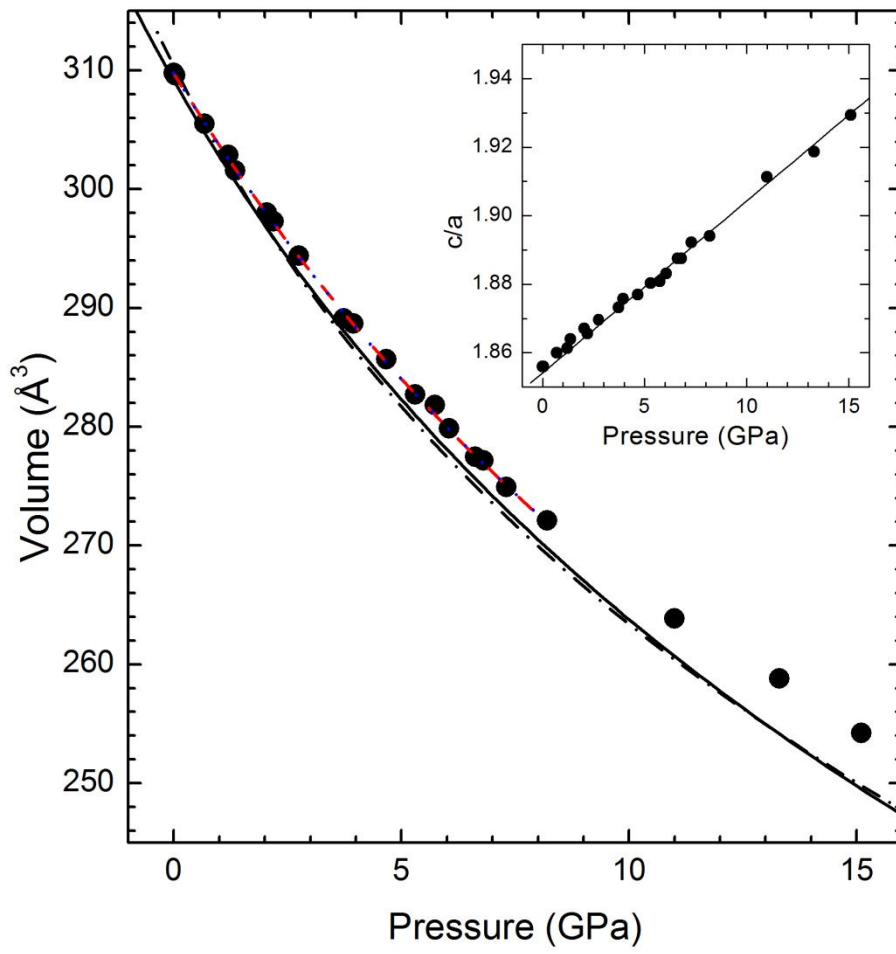
657 **Figure 2**



658

659

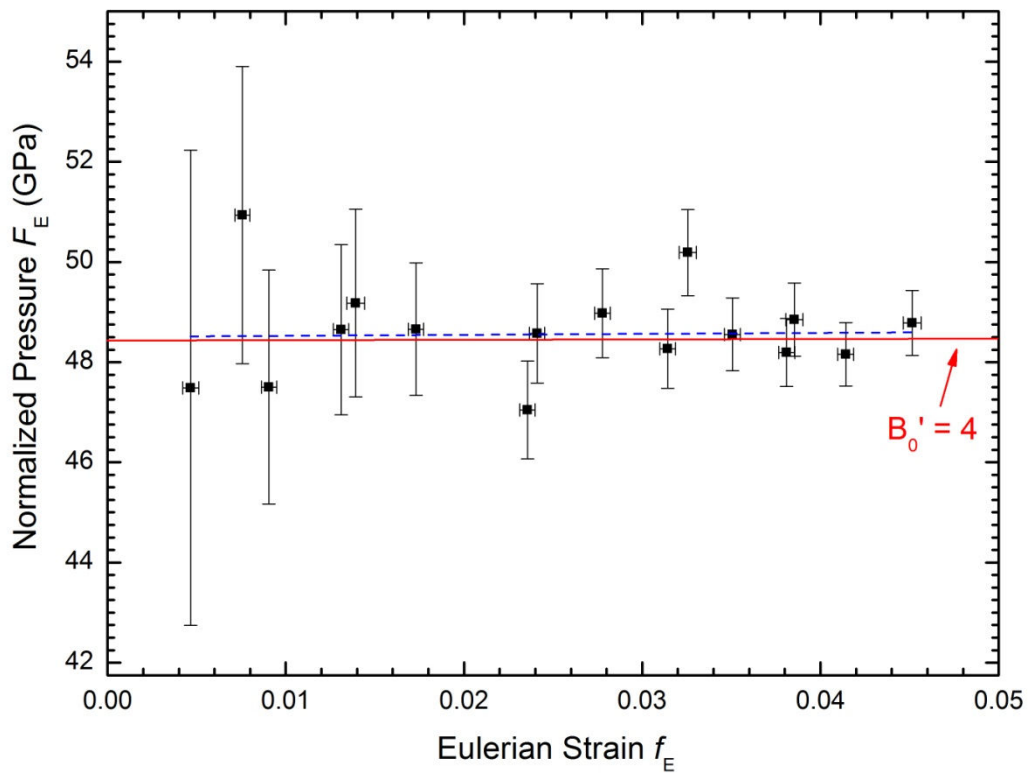
660 **Figure 3**



661

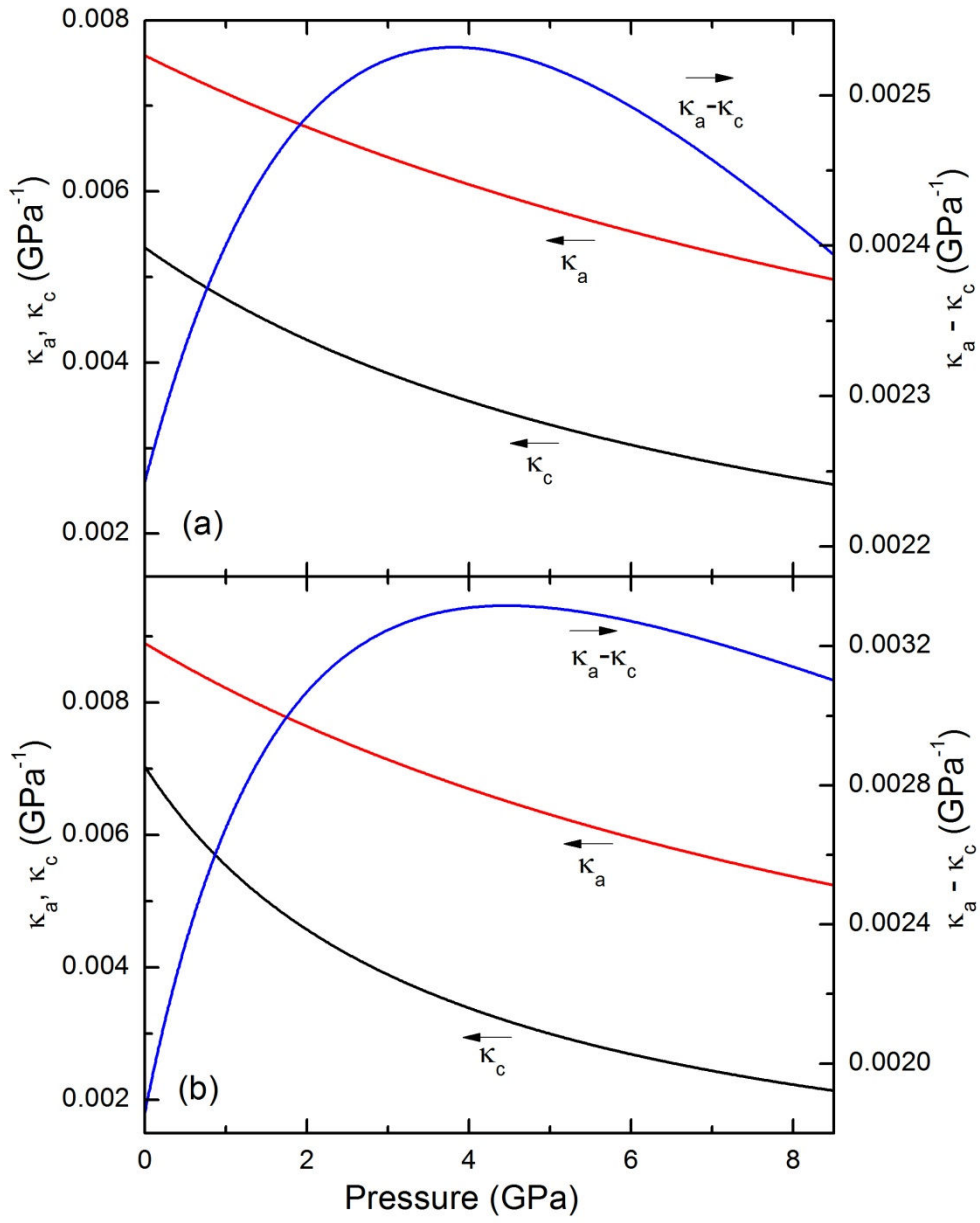
662

663 **Figure 4**
664



665
666

667 **Figure 5.**



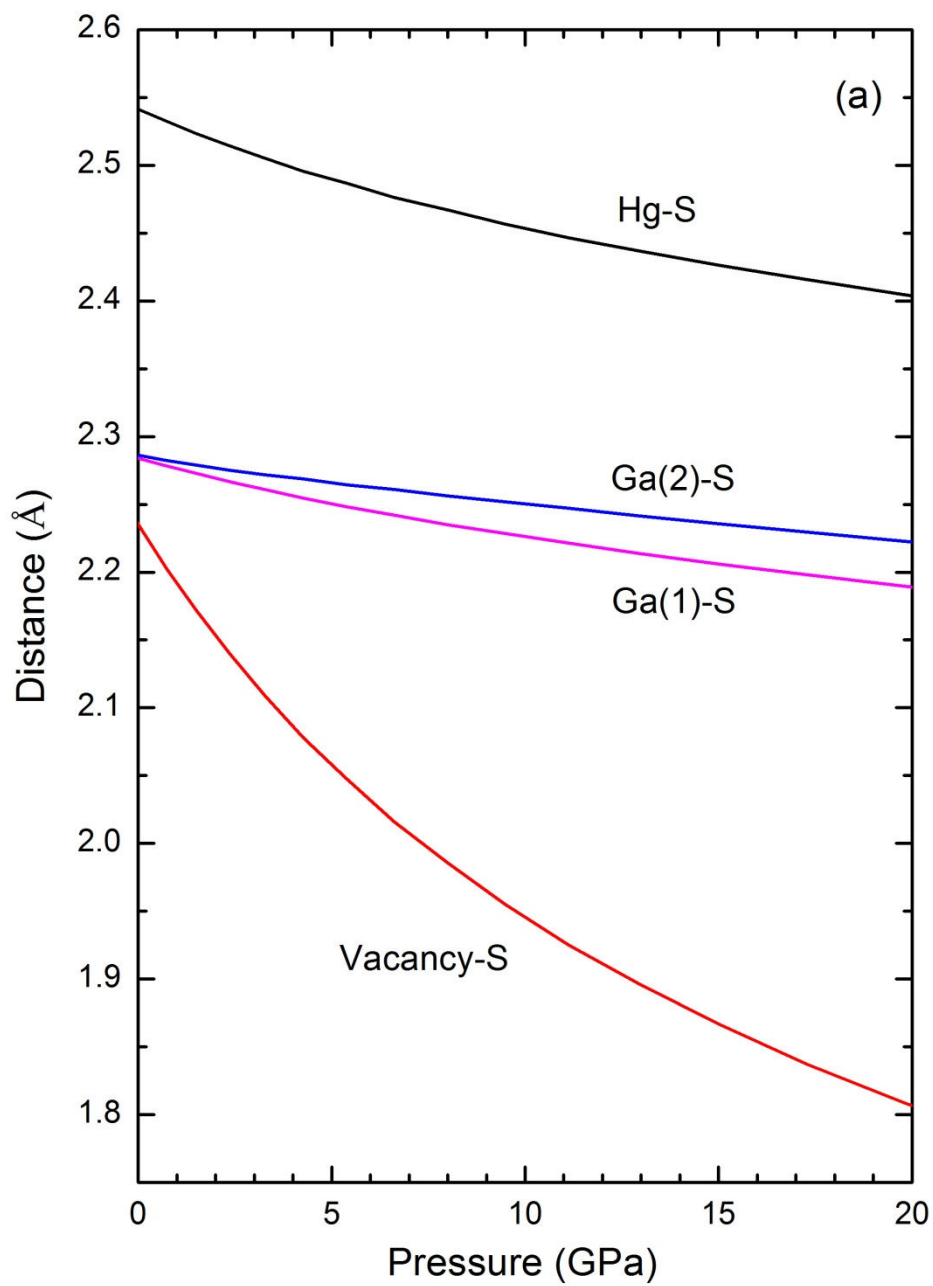
668

669

670

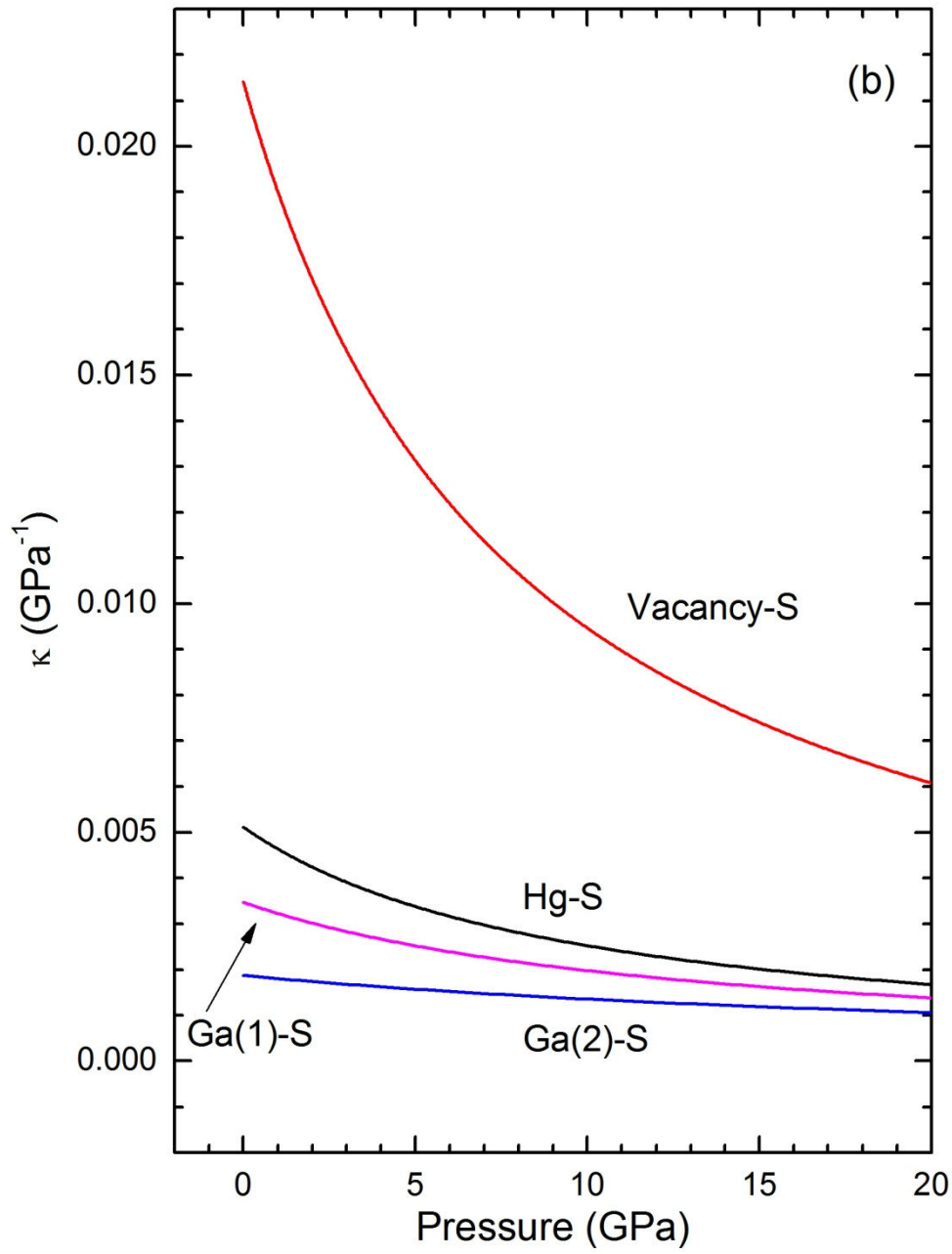
671 **Figure 6a.**

672



673
674

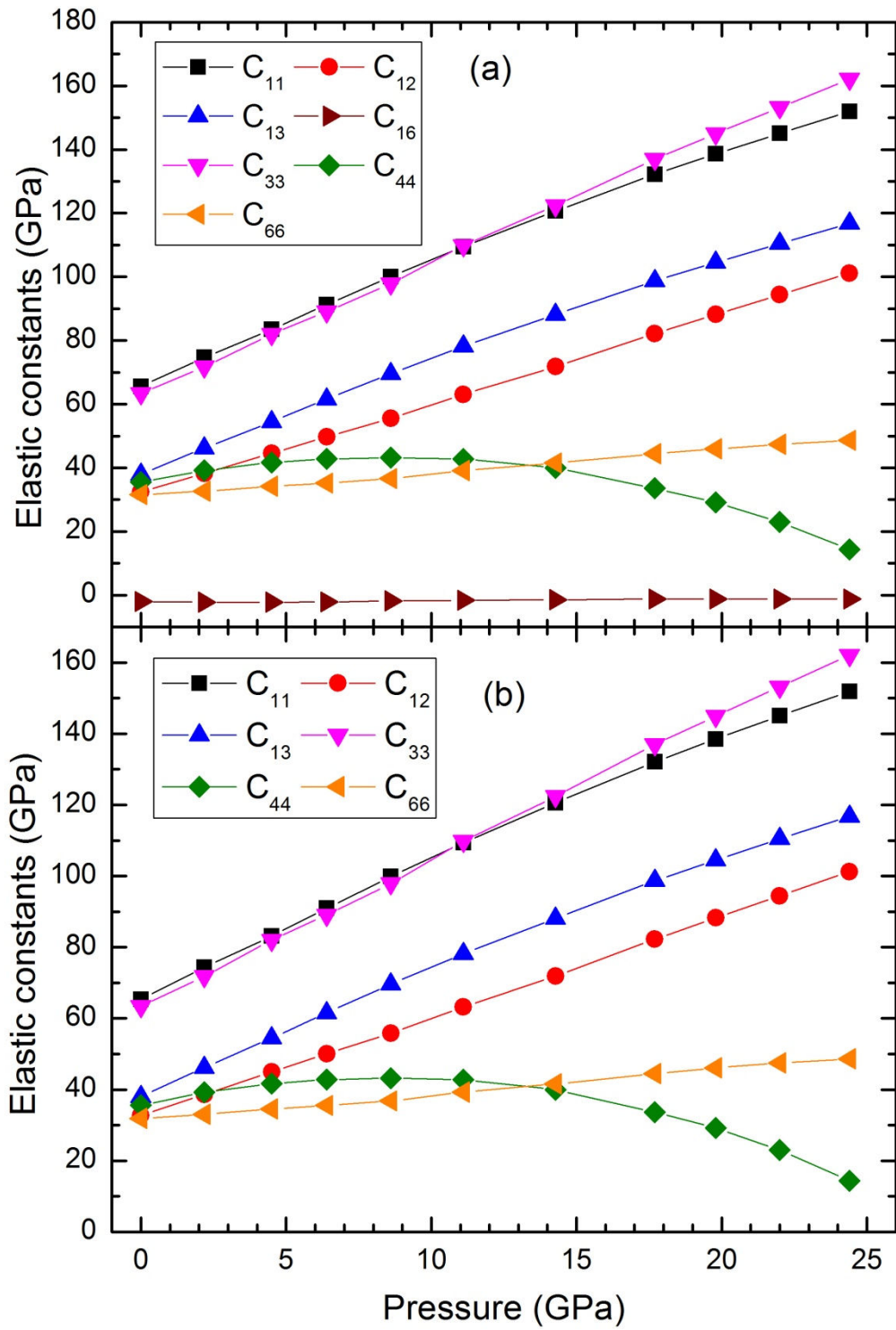
675 **Figure 6b.**



676

677

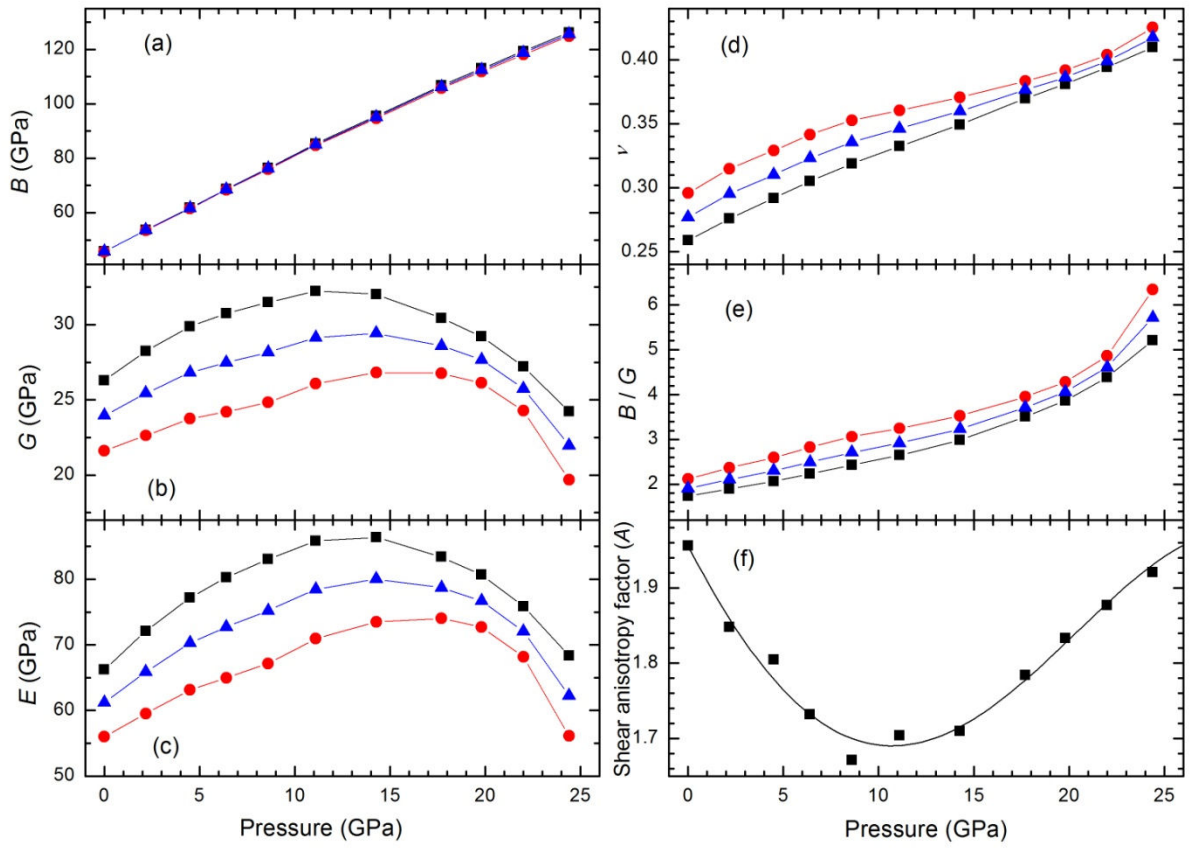
678 **Figure 7.**



679

680

681 **Figure 8.**



682

683

684

685